Dalton Transactions

ROYAL SOCIETY OF CHEMISTRY

PAPER

View Article Online
View Journal | View Issue

Cite this: *Dalton Trans.*, 2026, **55**, 8314

Luminescence of BaFBr nanoplates codoped with $Eu^{2+/3+}$

Nishani T. Manamperi, S. Sameera Perera and Federico A. Rabuffetti *

$BaFBr:Eu^{2+/3+}$ monodisperse nanocrystals were synthesized *via* solution-phase thermolysis of metal bromodifluoroacetates. Their luminescence response was characterized between 80 and 430 K. Nanocrystals exhibited square-plate shape with approximate dimensions 33 nm × 5 nm and polydispersities below 8% in both dimensions. The emission spectrum of $BaFBr:Eu^{2+/3+}$ featured a broad band in the near UV arising from fd–f transitions of Eu^{2+} as well as a series of line-like bands from f–f transitions of Eu^{3+}. No line emission from the $4f^7$ ($^6P_{7/2}$) level of Eu^{2+} was observed. The structure and dynamics of the excited states involved in Eu^{2+} violet emission were established from the temperature dependence of their time-resolved decays. The lifetime of the $4f^65d^1$ excited-state manifold exhibited antithermal quenching between 80 and 430 K. This observation could not be rationalized invoking thermalization of the lowest level of the $4f^65d^1$ manifold to the higher-lying $4f^7$ ($^6P_{7/2}$) level. A satisfactory explanation was achieved considering thermal coupling between the lowest level of the $4f^65d^1$ manifold and a higher-lying $4f^65d^1$ level. The latter featured a smaller radiative rate than the former (≈10^5 *vs.* 10^6 s^{-1}) and the gap between these two levels was estimated to be ≈500 cm^{-1}. The $4f^7$ ($^6P_{7/2}$) level was located ≈100 cm^{-1} above the higher-lying $4f^65d^1$ level and, unlike the case of BaFCl, did not need to be invoked at all to rationalize the temperature dependence of Eu^{2+} emission.

Received 11th March 2026,
Accepted 30th April 2026

DOI: 10.1039/d6dt00603e

rsc.li/dalton

Introduction

Alkaline-earth fluorohalides of formula MFX (M = Ca, Sr, Ba; X = Cl, Br, I) have been extensively used as hosts for divalent and trivalent rare-earth ions (*e.g.*, $Sm^{2+/3+}$, $Eu^{2+/3+}$, Er^{3+}, Tm^{3+}, Yb^{3+}). Isovalent and aliovalent doping of these wide bandgap insulators renders them photoluminescent and photosensitive functional materials. Pressure[1–3] and temperature[4–6] luminescent sensors, scintillators,[7] photostimulable X-ray storage phosphors,[8–10] and photoexcitable storage phosphors sensitive to X-ray and UV-C radiation have thus been realized.[11–17] Besides leveraging the chemical and structural tunability of these materials to tailor their optical response, there is continued interest in understanding the impact of crystal morphology—specifically of crystal size—on their photophysics and photochemistry.[11,13,17–20]

As a part of that effort, our group recently reported on the luminescence of $BaFCl:Eu^{2+/3+},Tb^{3+}$ nanocrystals synthesized *via* hot-injection.[21] Although trivalent europium was used as a reagent and no reducing agent was intentionally introduced in the reaction mixture, partial reduction to divalent europium occurred during synthesis. Incorporation of Eu^{2+} into micro and nanocrystalline BaFX has been extensively reported but solids were invariably synthesized using a divalent europium precursor (*e.g.*, EuF_2)[22,23] and/or a reducing atmosphere (*e.g.*, N_2/H_2, graphite powder).[22,24,25] The unexpected *in situ* reduction of Eu^{3+} to yield BaFCl nanocrystals codoped with Eu^{2+} and Eu^{3+} prompted us to investigate whether mixed-valence could also be achieved in nanocrystalline BaFBr under similar synthetic conditions. Additionally, we were interested in revisiting the structure and dynamics of the excited states of Eu^{2+} in BaFBr. To the best of our knowledge, there is only one experimental investigation on this topic, reported by Spoonhower and Burberry and conducted on single-crystalline $BaFBr:Eu^{2+}$.[24] The structure and temperature-dependent dynamics of Eu^{2+} derived by these authors was later questioned by Meijerink and Blasse;[26] however, no follow-up studies were carried out to test the validity of the alternative model proposed by the latter.

In this article, we report a study of the luminescence of monodisperse $BaFBr:Eu^{2+/3+}$ nanoplates synthesized *via* hot-injection. Excitation and emission were probed at room temperature and the temperature-dependent emission profiles of Eu^{2+} and Eu^{3+} were characterized between 80 and 430 K. In the case of Eu^{2+}, time-resolved variable-temperature luminescence decays were quantitatively analyzed to probe the structure and dynamics of the excited states responsible for near UV emission. Results are discussed in the context of what has been pre-

Department of Chemistry, Wayne State University, Detroit, MI 48202, USA.
E-mail: far@chem.wayne.edu

viously reported for bulk and nanocrystalline Eu^{2+}-doped BaFBr and BaFCl.

Experimental

Synthesis of BaFBr:$Eu^{2+/3+}$ nanoplates

Nanocrystal synthesis was conducted using standard Schlenk techniques under nitrogen atmosphere. Reagents included $BaCO_3$ (0.95 mmol, 99.98%, Sigma-Aldrich), Eu_2O_3 (0.025 mmol, 99.9%, Sigma-Aldrich), CF_3COOH (1 mL, 99%, Sigma-Aldrich), $CF_2BrCOOH$ (2 mmol, 97%, Synquest Laboratories), oleic acid (2 mL, 90%, Sigma-Aldrich), 1-octadecene (2 mL, 90%, Sigma-Aldrich), trioctylphosphine (8 mL, 97%, Sigma-Aldrich), and double-deionized water (5 mL). All reagents were used as received. BaFBr:Eu nanoplates (5 mol% nominal, doping efficiency *ca.* 80%) were synthesized and isolated following a hot-injection route and a work-up procedure described in detailed elsewhere.[17] The two-step hot-injection route entailed preparation of metal bromodifluoroacetate precursors *via* solvent evaporation[5] followed by thermolysis in high-boiling point organic solvents. Polycrystalline samples thus obtained appeared off-white in color and were employed in structural, morphological, and luminescence studies.

Powder X-ray diffraction (PXRD)

PXRD patterns were collected using a Bruker D2 Phaser diffractometer operated at 30 kV and 10 mA. Cu Kα radiation (λ = 1.5418 Å) was employed. A nickel filter was used to remove Cu Kβ radiation. Diffractograms were collected in the 10–60° 2θ range using a step size of 0.012° and a step time of 1.1 s unless noted otherwise.

Rietveld analysis

Rietveld analysis[27,28] of PXRD data was conducted using the General Structure Analysis System II (GSAS-II).[29] The following parameters were refined: (i) scale factor and sample displacement; (ii) background, which was modeled using a shifted Chebyschev function; (iii) lattice constants; (iv) atomic coordinates when allowed by space-group symmetry (*P*4/*nmm*); and (v) crystallite size and microstrain. Isotropic displacement parameters were fixed at 0.01, 0.03, and 0.02 $Å^2$ for Ba, F, and Br, respectively. The quality of the refined structural model was assessed using the value of the R_w residual and the difference between the observed and calculated intensities divided by the standard uncertainty of the observed intensities ($\Delta(I)/\sigma(I)$).

Transmission electron imaging (TEM)

TEM images were obtained using a Thermo Scientific Talos F200X G2 S/TEM microscope operated at 200 kV. A small aliquot of the native solution containing BaFBr:Eu nanocrystals was mixed with toluene and dropcast onto a 200-mesh Cu grid coated with a lacey carbon film (Ted Pella Inc.). Size distribution histograms were obtained after analyzing 150 nanocrystals.

X-ray photoelectron spectroscopy (XPS)

XPS spectra were collected using a Thermo Scientific Nexsa X-ray photoelectron spectrometer equipped with a hemispherical analyzer and monochromatic Al Kα sources (1486.7 eV). ≈10 mg of polycrystalline BaFBr:Eu were mounted on a regular sample holder using conductive copper tapes; care was taken to ensure a flat surface. The holder was then loaded into the entry-lock chamber and held under vacuum for more than 30 min. Once the vacuum level reached 4×10^{-7} mbar, the sample was transferred from the entry-lock to the analysis chamber, which was kept at a base pressure of $\approx 2.3 \times 10^{-7}$ mbar throughout data acquisition. High-resolution spectra were collected for C 1s, Eu 3d, and Ba 3p core lines using a pass energy of 50 eV, an energy step size of 0.1 eV, and 100 ms per step as the dwell time. Spectral analyses were performed using Thermo Avantage. The C 1s core line at 284.8 eV was employed for charge referencing. All peaks were fitted using pseudo-Voigt functions.

Spectrofluorometry

Luminescence analyses were conducted using a Fluorolog 3-222 fluorometer (Horiba Scientific). A xenon lamp was used as the excitation source for acquisition of steady-state spectra. A 260 nm DeltaDiode and a 265 nm SpectraLED (Horiba Scientific) were used for collection of time-resolved luminescence decays. A photomultiplier tube R928 (Hammamatsu Photonics) served as the detector. BaFBr:Eu nanocrystals were loaded into a VPF-800 variable-temperature stage (Lake Shore Cryotronics). Spectra and decays were first collected under ambient conditions and then variable-temperature measurements were conducted. For the later, nanocrystals were heated at 450 K for 2 h under vacuum (≈50 mTorr) prior to data collection. Spectra and decays were collected in the 80–430 K temperature window using a band-pass of 1 nm. Nanocrystals were allowed to dwell for ≈20 min at the target temperature prior to data acquisition. Temperature control was provided by a Lake Shore 335–3060 controller. A heating rate of 10 K min^{-1} was employed throughout. All spectrofluorometric analyses were conducted using polycrystalline solids that had not been exposed to X-ray radiation.

UV-vis diffuse reflectance spectroscopy

Diffuse reflectance spectra were collected between 200 and 800 nm using a Jasco V570 UV-vis-NIR spectrophotometer featuring a 60 mm integrating sphere. $BaSO_4$ (99.99%, Sigma-Aldrich) was used as a reflectance standard. Reflectance (R) was converted to absorbance using the Kubelka–Munk function $F(R)$ according to $F(R) = (1 - R)^2/2R$.[30]

Results and discussion

The phase purity and morphology of BaFBr:Eu nanocrystals were probed using PXRD and TEM, respectively. A diffraction pattern and representative microscopy images are given in

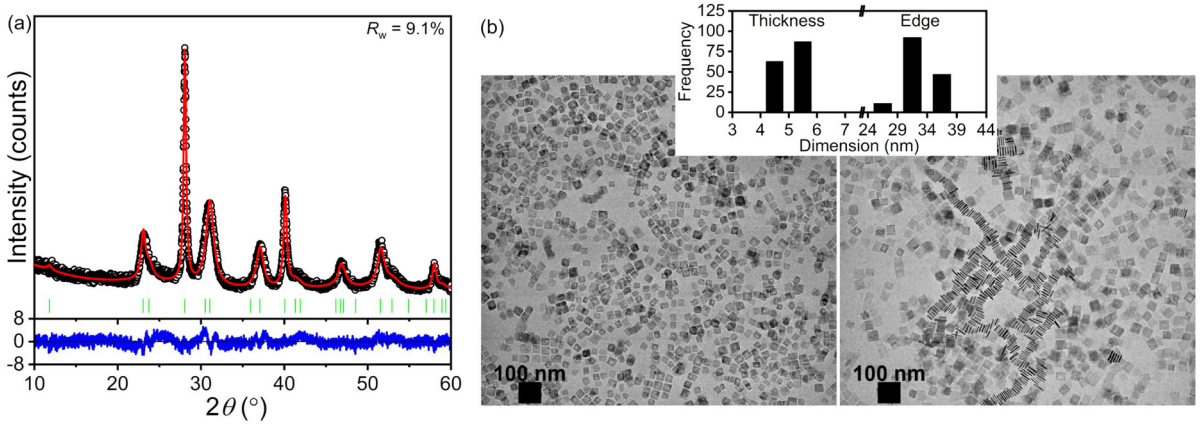

Fig. 1 (a) Rietveld analysis of the PXRD pattern of BaFBr:$Eu^{2+/3+}$. Experimental (black circles) and calculated patterns (red line), $\Delta(I)/\sigma(I)$ curve (blue line), and tick marks (green vertical bars) corresponding to the calculated diffraction maxima are shown. (b) Representative TEM images of BaFBr:$Eu^{2+/3+}$. Inset: size distribution histograms obtained after measuring 150 side-lying and edge-lying nanoplates.

Fig. 1. The phase purity of polycrystalline BaFBr:Eu was confirmed by a Rietveld analysis. All diffraction maxima were indexed to the fluorobromide phase (PDF No. 024–0090); no secondary crystalline phases were observed (Fig. 1a). Refined unit cell constants, atomic coordinates, and bond distances are given in the SI (Table S1). Diffraction maxima exhibited anisotropic microstrain broadening that complicated adequate modeling of some reflections (*e.g.*, $2\theta \approx 23.3°$ (101), 23.9° (002), 30.7° (111), and 37.1° (112)). Nanocrystals exhibited square-plate shape with an average edge length of 32.7 (2.4) nm and an average thickness of 5.0(3) nm (Fig. 1b). Polydispersities below 8% were achieved in both dimensions, demonstrating that our hot-injection route affords monodisperse nanocrystals. The combination of phase purity, narrow size distribution, and uniform shape is ideal to ensure the statistical significance of structure–photophysics relationships derived from probing the nanocrystal ensemble.

The room-temperature luminescence response of the as-prepared nanoplates was probed with the goal of establishing whether reduction of Eu^{3+} to Eu^{2+} occurred during synthesis, as it was the case with BaFCl.[21] Results from these studies are summarized in Fig. 2. An emission spectrum collected under 275 nm excitation revealed, indeed, the presence of Eu^{2+} and Eu^{3+} as emitting centers (Fig. 2a). The spectrum was dominated by a broad band peaking at 392 nm arising from radiative relaxation of lowest level of the Eu^{2+} $4f^65d^1$ excited-state manifold ($4f^65d^1$ (*ll*) hereafter) to the $4f^7$ ($^8S_{7/2}$) ground state. Unlike what was reported by us and others for Eu^{2+}-doped BaFCl,[21,25,31–34] line emission from the zero-phonon transition $4f^7$ ($^6P_{7/2}$) → $4f^7$ ($^8S_{7/2}$) was not observed, indicating that in BaFBr the $4f^65d^1$ (*ll*) excited state sits below the $4f^7$ ($^6P_{7/2}$) level (see inset of Fig. 2a). Besides Eu^{2+} emission, weaker emissions from $4f^6$ ($^5D_0$) → $4f^6$ (^7F_J) transitions of Eu^{3+} were observed at 593 (J = 1), 613 (J = 2), 651 (J = 3), and 700 nm (J = 4). The presence of Eu^{2+} and Eu^{3+} was further confirmed by time-resolved luminescence decays (Fig. 2b and c). Intensity-

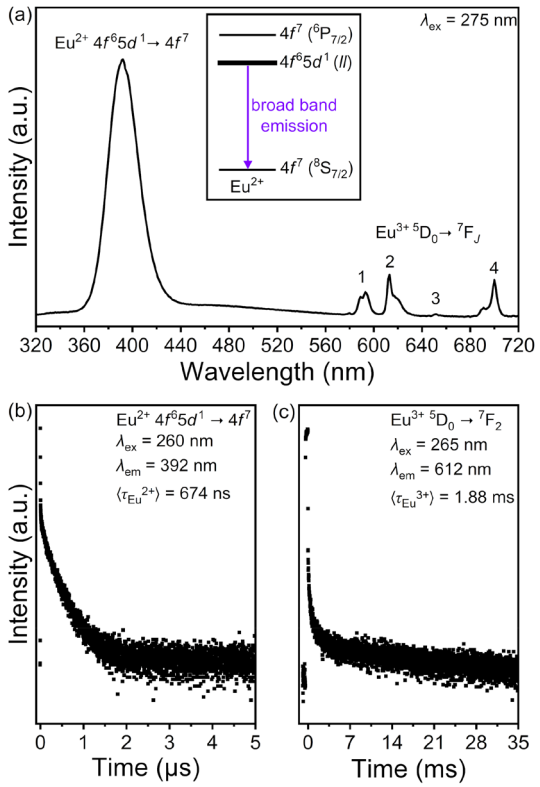

Fig. 2 Room-temperature emission spectrum (a) and time-resolved luminescence decays of BaFBr:$Eu^{2+/3+}$ (b, c). A qualitative energy diagram depicting the lowest-energy section of the excited-state manifold of Eu^{2+} is provided in the inset of (a). Decays in (b, c) are plotted in logarithmic scale.

weighted average lifetimes (τ) were estimated using eqn (1), where $I(t)$ is

$$\tau = \frac{\int I(t)t\mathrm{d}t}{\int I(t)\mathrm{d}t} \quad (1)$$

the baseline-corrected luminescence intensity at time t. Integration was carried out from the first point of the decay until its return to the baseline level. Lifetimes equal to 0.67 μs and 1.88 ms were thus obtained for Eu^{2+} ($4f^6 5d^1$ (ll) → $4f^7$) and Eu^{3+} ($^5D_0 \rightarrow {}^7F_2$), respectively. The excited-state lifetime of Eu^{2+} was in line with estimates previously reported for bulk and nanocrystalline BaFBr:Eu^{2+}, all of which were in the sub-microsecond range.[24,35–38] Lifetimes obtained for Eu^{2+} and Eu^{3+} were significantly shorter than those reported for the same emissions in BaFCl nanocrystals of comparable size (26 μs for Eu^{2+} and 3.3 ms for Eu^{3+}).[21] Altogether, results from luminescence screening showed that synthesis conditions employed in our hot-injection approach to BaFCl and BaFBr nanocrystals generate a chemical species capable of driving the partial reduction of Eu^{3+} to its divalent form; at present, we are unable to identify this species.

We attempted to estimate the Eu^{2+} : Eu^{3+} ratio in BaFBr:Eu nanoplates using XPS. Results from these analyses are shown in Fig. 3. The high-resolution Eu 3d spectrum exhibited peaks in the $3d_{5/2}$ and $3d_{3/2}$ regions and a complex shape due to the presence of shake-up and shake-down features. Well-established peak-fit guidelines[39–41] enabled peak deconvolution and extraction of quantitative information. The spectrum was dominated by an intense peak at ≈1136.9 eV. This peak was deconvoluted into Ba $3p_{1/2}$ and Eu $3d_{5/2}$ contributions while maintaining the area ratio of 1 : 2 between the Ba $3p_{3/2}$ and Ba $3p_{1/2}$ spin–orbit components (Ba $3p_{3/2}$ component centered at ≈1063.4 eV is not shown in Fig. 3). Deconvolution resulted in two peaks centered at ≈1135.2 and ≈1137.0 eV assigned to Eu $3d_{5/2}$ (Eu^{3+}) and Ba $3p_{3/2}$ core lines, respectively. Though the Eu $3d_{5/2}$ peak arising from Eu^{3+} overlapped with the Ba $3p_{1/2}$ peak, the Eu $3d_{3/2}$ peak centered at ≈1164.8 eV unequivocally confirmed the presence of Eu^{3+}. The presence of Eu^{2+} was confirmed by Eu $3d_{5/2}$ and Eu $3d_{3/2}$ peaks centered at ≈1125.2 and ≈1154.9 eV, respectively. The areas of the Eu $3d_{5/2}$ peaks corresponding to Eu^{2+} and Eu^{3+} were computed and translated to atomic percentages, which were subsequently used to estimate the Eu^{2+} : Eu^{3+} ratio. A value of 0.75 was thus obtained, indicating that ≈43% of the Eu^{3+} in the initial reaction mixture had been reduced to Eu^{2+} (n.b., assuming that the calculated ratio was representative of the entire nanocrystal volume). This value was lower than that obtained for BaFCl nanocrystals, in which the extent of reduction reached ≈56%.[21]

Room-temperature excitation spectra of BaFBr:Eu nanoplates were collected to probe whether selective excitation of Eu^{2+} or Eu^{3+} could be achieved. Results from these studies are presented in Fig. 4. Excitation spectra were collected monitoring emissions at 392 (Eu^{2+}) and 612 nm (Eu^{3+}), respectively (Fig. 4a). Both spectra looked similar to those obtained for BaFCl:$Eu^{2+/3+}$ nanocrystals.[21] The spectrum of Eu^{2+} 392 nm emission was dominated by a broad band with maxima at 265 and 275 nm plus a shoulder at 285 nm. We assign these maxima to transitions from the $4f^7$ ($^8S_{7/2}$) ground state to the upper levels of the $4f^6 5d^1$ excited state (*vide infra*).[9,42] In the case of Eu^{3+} 612 nm emission, the excitation spectrum featured a sharp maximum at 393 nm, arising from the $4f^6$

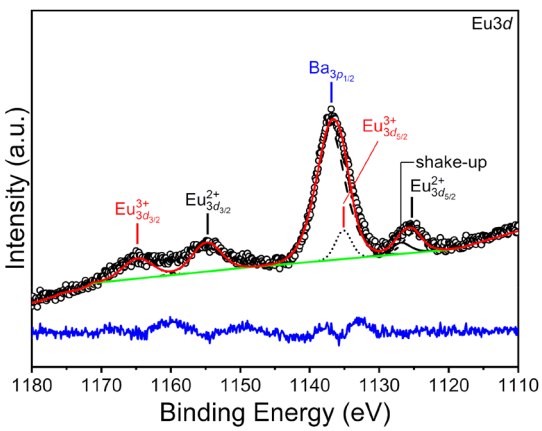

Fig. 3 High-resolution Eu 3d XPS spectrum of BaFBr:$Eu^{2+/3+}$. Experimental data (black circles), calculated spectrum (red line), background (green line), and difference curve (blue line, offset for clarity) are shown. Also shown are deconvoluted peaks corresponding to Eu^{2+} (short-dashed black line), Eu^{3+} (dotted black line), Ba 3p core (dashed black line), and shake-up features (solid black line).

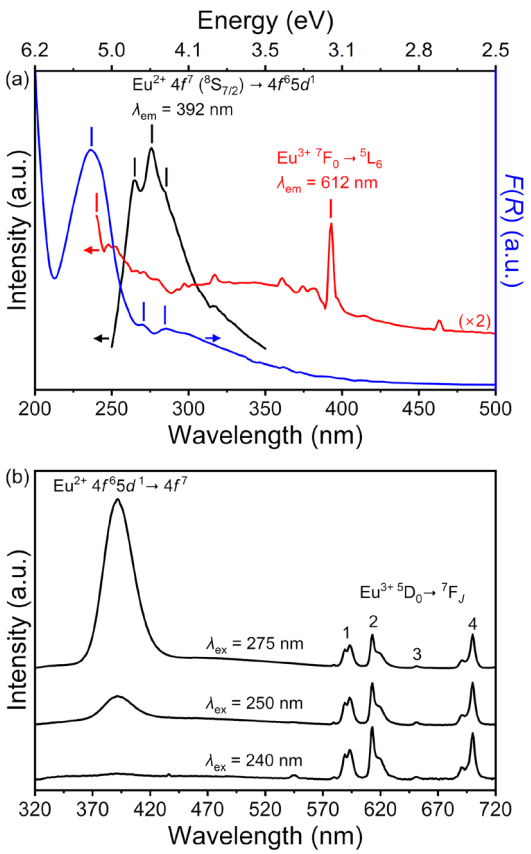

Fig. 4 (a) Excitation and absorption spectra of BaFBr:$Eu^{3+/2+}$. (b) Emission spectra collected with different excitation wavelengths. All spectra were collected at room temperature.

($^7F_0$) → 4f^6 ($^5L_6$) transition. Additionally, a broad band with maximum at 240 nm was observable, which we assign to a charge-transfer state from oxide defects to the ground state of Eu^{3+} (*i.e.*, $O^{2-} + Eu^{3+}$ ($^7F_0$) → $O^- + Eu^{2+}$ ($^8S_{7/2}$)).[43] Incorporation of oxygen in the fluorohalide lattice is well-documented and unavoidable during synthesis.[44–47] Finally, we note the absence of efficient excitation of Eu^{3+} at 275 nm, where the center of the Eu^{2+} 4f^7 ($^8S_{7/2}$) → 4f^{6}5d^1 band was located. Thus, sensitization of Eu^{3+} by Eu^{2+} did not occur to an appreciable extent. The absorption spectrum of BaFBr:Eu nanoplates confirmed the abovementioned assignments. The onset of absorption was observed around 388 nm (3.20 eV), close to the position of the lowest level of the 4f^{6}5d^1 excited state (≈3.35 eV, *vide infra*). Absorption of Eu^{2+} *via* the 4f^7 ($^8S_{7/2}$) → 4f^{6}5d^1 transition extended into the UV region, where maxima at 270 and 285 nm (4.59 and 4.35 eV, respectively) were observed. These absorption bands are characteristic of Eu^{2+} doped into BaFBr[48] and their positions closely matched those of maxima observed in the excitation spectrum. Besides bands arising from Eu^{2+}, the absorption spectrum featured an intense and broad band peaking at 237 nm (5.23 eV). This band is a signature of oxide defects in BaFBr and BaFCl, which are known to absorb below 250 nm (5 eV),[13,44,47,49–51] and its position matched that of the maximum observed in the excitation spectrum of Eu^{3+}. The independent origin of the 240 and 270–285 nm absorption bands prompted us to investigate whether we could selectively excite Eu^{2+} or Eu^{3+}. To this end, emission spectra were collected under 275, 250, and 240 nm excitation. Increasing excitation energy favored Eu^{3+} emission (Fig. 4b). Emissions from both Eu^{2+} and Eu^{3+} occurred upon excitation at 275 nm (4.51 eV), with the former dominating the spectrum. By contrast, excitation at 240 nm (5.17 eV) led to emission from Eu^{3+} only. A comparison of the wavelength-dependence of the emission spectra of BaFBr and BaFCl nanocrystals codoped with Eu^{2+} and Eu^{3+} showed that Eu^{3+} emission in both hosts was favored upon increasing excitation energy; that is, upon moving from excitation of Eu^{2+} *via* the 4f^7 ($^8S_{7/2}$) → 4f^{6}5d^1 transition to Eu^{3+} excitation *via* oxide defect absorption. However, the spectral responses of BaFBr and BaFCl differed in terms of the wavelength at which each activator could be selectively excited. In BaFBr, Eu^{3+} could be selectively excited at 240 nm, whereas excitation at 275 nm led to emissions from both Eu^{3+} and Eu^{2+}. Conversely, Eu^{2+} in BaFCl could be selectively excited at 275 nm, whereas excitation at 240 nm led to emissions from both activators.

Finally, variable-temperature luminescence studies were conducted with the aim of establishing the structure and dynamics of Eu^{2+} excited states involved in broad band violet emission. Emission spectra and time-resolved decays were collected between 80 and 430 K after thermally treating BaFBr:$Eu^{2+/3+}$ nanoplates as described in the Experimental section. Thermal treatment had no effect on chemical and structural integrity as shown by X-ray diffraction and thermal analysis (see SI, Fig. S1). Results from variable-temperature studies are summarized in Fig. 5. Emission spectra collected under 275 nm excitation confirmed that the 4f^{6}5d^1 (*ll*) excited state

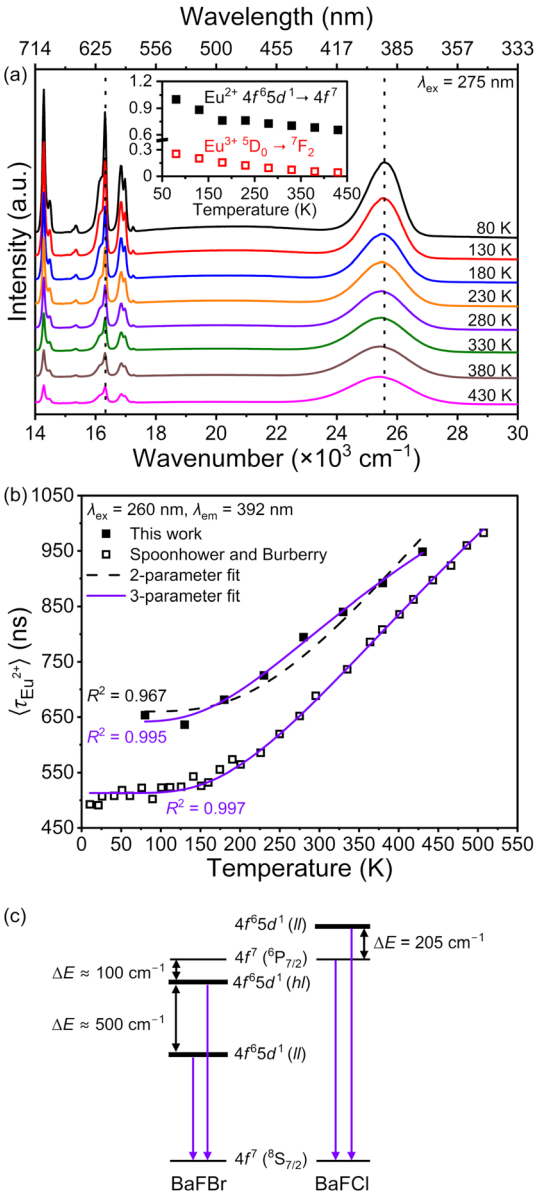

Fig. 5 (a) Variable-temperature emission spectra of BaFBr:$Eu^{2+/3+}$. The temperature dependence of the integrated intensities of Eu^{2+} and Eu^{3+} emission bands depicted with dotted lines is shown in the inset. (b) Temperature-dependence of the average lifetime of Eu^{2+} excited-state manifold. Experimental lifetimes from this work and Spoonhower and Burberry's are shown. Two- and three-parameter fits of eqn (2) to experimental data are given along with fit residuals. (c) Quantitative energy diagrams illustrating the lowest-energy section of the excited-state manifold of Eu^{2+} in BaFBr (this work) and BaFCl nanocrystals of comparable size (data from ref. 21). The 4f^7 ($^6P_{7/2}$) level is located at 27 600 cm^{-1}. Purple arrows depict radiative transitions responsible for Eu^{2+} violet emission.

of Eu^{2+} sits below the 4f^7 ($^6P_{7/2}$) level. Indeed, no line emission from the latter was observed at temperatures as low as 80 K (Fig. 5a). Noteworthy was the fact that ratio between the integrated intensities of the 4f^{6}5d^1 (*ll*) → 4f^7 (≈25 570 cm^{-1}) and $^5D_0$ → $^7F_2$ (≈16 340 cm^{-1}) emission bands of Eu^{2+} and Eu^{3+},

respectively, increased with temperature. Although the opposite trend was expected on the basis of the strength of electron–phonon coupling in fd and f states, the increase in the width of the Eu^{2+} emission band drove the value of the ratio from ≈4 at 80 K to ≈16 at 430 K. For completeness, we checked whether that ratio could be used for luminescence thermometry purposes; however, only modest temperature sensitivity values were achieved in a preliminary screening (0.54% K^{-1} at 271 K, see SI, Fig. S2). We then focused on estimating the photophysical parameters of the excited-state manifold of Eu^{2+} using the temperature dependence of its average decay time $\langle\tau_{Eu^{2+}}\rangle$. Luminescence decays excited at 260 nm and monitored at 392 nm were used to extract intensity-weighted average lifetimes according to eqn (1) (*vide supra*); experimental decays are given in the SI (Fig. S3). Numerical differences aside, the temperature dependence of $\langle\tau_{Eu^{2+}}\rangle$ in our BaFBr:$Eu^{2+/3+}$ nanoplates closely matched that observed by Spoonhower and Burberry in single-crystalline BaFBr:Eu^{2+} (Fig. 5b). This similarity demonstrated that the dynamics of Eu^{2+} excited-state manifold was not affected by the presence of Eu^{3+} and of a presumably higher concentration of oxide defects. In the case of nanoplates, the average lifetime of the excited-state manifold increased from 653 ns at 80 K to 949 ns at 430 K. No signs of thermal quenching were visible within that temperature range. Although unusual, an increase in the excited-state lifetime of Eu^{2+} has been previously observed in a number of hosts, including CaF_2,[52–54] $Ba_5SiO_4Br_6$,[26] and BaFBr itself.[24] Qualitatively, antithermal quenching may be explained invoking the presence of a higher-lying excited state thermally coupled to $4f^65d^1$ (*ll*) and whose decay probability to the $4f^7$ ($^8S_{7/2}$) ground state is smaller than that of the latter.[52] In the case of BaFBr:Eu^{2+}, Spoonhower and Burberry acknowledged the presence of a "less-radiative" higher-lying excited state. In analogy with what had been done for Eu^{2+}-doped SrFCl and BaFCl,[25,31,33] these authors modeled the temperature dependence of $\tau_{Eu^{2+}}$ using a three-level system. The corresponding analytical expression of $\tau_{Eu^{2+}}(T)$ is given in eqn (2), which was proposed by Feofilov and Tolstoi.[55] Here, $k_{Eu^{2+}}$ is the effective radiative constant of the excited-state manifold, k_{ll} and k_{hl} are the radiative constants of the lower-lying and higher-lying excited levels, respectively, g_{ll} and g_{hl} their corresponding degeneracies, ΔE the energy difference between them, and k is Boltzmann's constant. Using this model, Spoonhower and Burberry reproduced the experimental temperature dependence of $\tau_{Eu^{2+}}$ under the following two assumptions: (i) the lower- and higher-lying levels corresponded to $4f^65d^1$ (*ll*) and $4f^7$ ($^6P_{7/2}$), respectively; and (ii) the radiative probability of the higher-lying level was zero (k_{hl} = 0). Additionally, they fixed the degeneracy ratio (g_{hl}/g_{ll} = 4), thus leaving k_{ll} and ΔE as adjustable parameters. This two-parameter model, however, failed to reproduce our experimental data (Fig. 5b). This prompted us to include the radiative constant of the higher-lying level as an adjustable parameter. A much better fit was achieved using this three-parameter model (Fig. 5b). The corresponding fit parameters were ΔE = 481(27) cm^{-1}, k_{ll} = 1.56(2) × 10^6 s^{-1}, and k_{hl} = 4.3(6) × 10^5 s^{-1}. The value of k_{ll} was in line with that expected for a parity-allowed fd → f transition (≈10^6 s^{-1}). On the other hand, the value of k_{hl} was abnormally larger than that expected for the parity-(and spin)-forbidden transition $4f^7$ ($^6P_{7/2}$) → $4f^7$ ($^8S_{7/2}$) (≈10^3–10^4 s^{-1}); such a value would have been expected for an fd → f transition.[56] The implications of this result were twofold. Firstly, it showed that the assumption of a nonradiative higher-lying level was not justified. In fact, a three-parameter model adequately reproduced Spoonhower and Burberry's data (Fig. 5b; ΔE = 499(10) cm^{-1}, k_{ll} = 1.95(1) × 10^6 s^{-1}, and k_{hl} = 5.4(3) × 10^5 s^{-1}). In addition, it demonstrated that assignment of the higher-lying level to the $4f^7$ ($^6P_{7/2}$) state was likely incorrect. Inconsistencies in Spoonhower and Burberry's explanation for antithermal quenching in BaFBr:Eu^{2+} had also been pointed out by Meijerink and Blasse upon analyzing temperature-dependent lifetime data for $Ba_5SiO_4Br_6$:Eu^{2+}.[26] Ultimately, the three-level system used to estimate the $4f^65d^1$ (*ll*)–$4f^7$ ($^6P_{7/2}$) energy gap in Eu^{2+}-doped SrFCl and BaFCl could not be applied to BaFBr. In the latter, the $4f^7$ ($^6P_{7/2}$) level sits above the $4f^65d^1$ (*ll*) level and its emission is masked by that of higher-lying levels of the $4f^65d^1$ excited-state manifold ($4f^65d^1$ (*hl*) hereafter) that are in thermal equilibrium with the lower-lying level $4f^65d^1$ (*ll*). In this framework, ΔE in eqn (2) corresponds to the $4f^65d^1$ (*ll*)–$4f^65d^1$ (*hl*) energy gap. Values of 481 (27) and 535(152) cm^{-1} were obtained for this gap using three- and four-parameter models, respectively. In the latter, the ratio of degeneracies was allowed to vary, yielding k_{ll} = 1.56(2) × 10^6 s^{-1}, k_{hl} = 6.2(3.8) × 10^5 s^{-1}, and g_{hl}/g_{ll} = 6.8(9.0) as fit parameters and R^2 = 0.995 as residual. The value of the $4f^65d^1$ (*ll*)–$4f^65d^1$ (*hl*) energy gap (≈500 cm^{-1}) was used in conjunction with position of the $4f^65d^1$ (*ll*) and $4f^7$ ($^6P_{7/2}$) levels to generate a diagram of the excited-state manifold of Eu^{2+} in BaFBr (Fig. 5c). The position of the $4f^65d^1$ (*ll*) level was estimated from the onset of its emission band at 80 K (≈27 000 cm^{-1}, 3.35 eV), while that of the $4f^7$ ($^6P_{7/2}$) level is independent of the host lattice (≈27 600 cm^{-1}, 3.42 eV).[57] A gap of ≈600 cm^{-1} between the $4f^65d^1$ (*ll*) and $4f^7$ ($^6P_{7/2}$) levels was thus extracted, in close agreement with the value of ≈800 cm^{-1} proposed by Meijerink and Blasse upon reanalysis of Spoonhower and Burberry's data.[26] Comparison of the excited-state manifolds of BaFBr and BaFCl[21] helps to visualize the distinct temperature dependence exhibited by Eu^{2+} emission in these two hosts. In the case of BaFCl, a temperature increase thermalizes the lower level of the manifold ($4f^7$ ($^6P_{7/2}$)) to a higher-lying level with *larger* radiative probability ($4f^65d^1$ (*ll*)); thus, luminescence thermal quenching is observed. By contrast, in the case of BaFBr, increasing temperature thermalizes the lower level of the manifold ($4f^65d^1$ (*ll*)) to a higher-lying level with *smaller* radiative probability ($4f^65d^1$ (*hl*)), thereby leading to antithermal quenching.

$$\tau_{Eu^{2+}}(T) = [k_{Eu^{2+}}(T)]^{-1} = \left\{\frac{k_{ll} + k_{hl} \times (g_{hl}/g_{ll}) \times \exp[-\Delta E/(kT)]}{1 + (g_{hl}/g_{ll}) \times \exp[-\Delta E/(kT)]}\right\}^{-1} \quad (2)$$

Conclusions

The luminescence response of BaFBr:$Eu^{2+/3+}$ monodisperse nanoplates was characterized between 80 and 430 K using steady-state and time-resolved spectrofluorometry. Although no reducing agent was deliberately incorporated in the reaction mixture, partial reduction of Eu^{3+} to Eu^{2+} occurred during nanocrystal synthesis. The resulting Eu^{2+} : Eu^{3+} ratio was estimated to be 0.75, corresponding to a reduction of 43% of the starting Eu^{3+} ions. A three-level system was employed to rationalize the structure and temperature-dependent dynamics of the excited states involved in Eu^{2+} violet emission. Photophysical parameters extracted by fitting this model to time-resolved decays were consistent with thermalization of the lowest level of the $4f^6 5d^1$ excited-state manifold to a higher-lying $4f^6 5d^1$level upon increasing temperature. The latter featured a smaller radiative probability than the former; as a result, antithermal quenching occurred. Unlike what had been previously proposed by Spoonhower and Burberry,[24] thermal population of the $4f^7$ ($^6P_{7/2}$) level did not need to be accounted for to rationalize the temperature dependence of Eu^{2+} emission.

The structure of the excited-state manifold of Eu^{2+} derived in this work for BaFBr differs from that observed in BaFCl. In the latter, the $4f^7$ ($^6P_{7/2}$) level sits below the lowest level of the $4f^6 5d^1$ excited state. Thermal coupling between these two levels leads to the well-known transition from line-like to broadband emission observed in BaFCl upon increasing temperature, as well as to the expected decrease in excited-state lifetime.

Conflicts of interest

There are no conflicts of interest to declare.

Data availability

All the data used are provided in the article and the supplementary information (SI). Supplementary information: (1) additional results from Rietveld analysis of X-ray diffraction data, (2) results from thermal analysis, (3) additional results from steady-state variable-temperature studies, and (4) time-resolved variable-temperature luminescence decays. See DOI: https://doi.org/10.1039/d6dt00603e.

Acknowledgements

The authors would like to acknowledge the financial support of the National Science Foundation (DMR-2508002) and the Department of Chemistry at Wayne State University. They also thank the Lumigen Instrument Center at Wayne State University for the use of the powder diffractometer (National Science Foundation MRI-1427926), electron microscopy (National Science Foundation MRI-2018587), and photoelectron spectroscopy facilities (National Science Foundation MRI-1849578).

References

1 Y. R. Shen, T. Gregorian and W. B. Holzapfel, Progress in Pressure Measurements with Luminescence Sensors, *High Pressure Res.*, 1991, **7**, 73–75.
2 P. Comodi and P. F. Zanazzi, Improved Calibration Curve for the Sm^{2+}-BaFCl Pressure Sensor, *J. Appl. Crystallogr.*, 1993, **26**, 843–845.
3 B. Lorenz, Y. R. Shen and W. B. Holzapfel, Characterization of the New Luminescence Pressure Sensor SrFCl:Sm^{2+}, *High Pressure Res.*, 1994, **12**, 91–99.
4 S. S. Perera, K. T. Dissanayake and F. A. Rabuffetti, Alkaline-Earth Fluorohalide Nanocrystals for Upconversion Thermometry, *J. Lumin.*, 2019, **207**, 416–423.
5 B. D. Dhanapala, H. N. Munasinghe, K. T. Dissanayake, L. Suescun and F. A. Rabuffetti, Expanding the Synthetic Toolbox to Access Pristine and Rare-Earth-Doped BaFBr Nanocrystals, *Dalton Trans.*, 2021, **50**, 16092–16098.
6 B. D. Dhanapala, H. N. Munasinghe and F. A. Rabuffetti, Temperature-Dependent Luminescence of CaFCl:Yb,Er Upconverting Nanocrystals, *J. Lumin.*, 2021, **235**, 117974.
7 S. Otake, T. Kato, D. Nakauchi, N. Kawaguchi and T. Yanagida, Development of Eu:BaFCl Translucent Ceramic Scintillators, *J. Lumin.*, 2024, **275**, 120828.
8 M. Sonoda, M. Takano, J. Miyahara and H. Kato, Computed Radiography Utilizing Scanning Laser Stimulated Luminescence, *Radiology*, 1983, **148**, 833–838.
9 K. Takahashi, K. Kohda, J. Miyahara, Y. Kanemitsu, K. Amitani and S. Shionoya, Mechanism of Photostimulated Luminescence in BaFX:Eu^{2+} (X = Cl, Br) Phosphors, *J. Lumin.*, 1984, **31–32**, 266–268.
10 K. Takahashi, J. Miyahara and Y. Shibahara, Photostimulated Luminescence (PSL) and Color-Centers in BaFCl-Eu^{2+}, BaFBr-Eu^{2+}, BaFI-Eu^{2+} Phosphors, *J. Electrochem. Soc.*, 1985, **132**, 1492–1494.
11 H. Riesen and W. A. Kaczmarek, Efficient X-ray Generation of Sm^{2+} in Nanocrystalline BaFCl/Sm^{3+}: A Photoluminescent X-ray Storage Phosphor, *Inorg. Chem.*, 2007, **46**, 7235–7237.
12 N. Riesen, A. François, K. Badek, T. M. Monro and H. Riesen, Photoreduction of Sm^{3+} in Nanocrystalline BaFCl, *J. Phys. Chem. A*, 2015, **119**, 6252–6256.
13 H. Riesen, K. Badek, T. M. Monro and N. Riesen, Highly Efficient Valence State Switching of Samarium in BaFCl:Sm Nanocrystals in the Deep UV for Multilevel Optical Data Storage, *Opt. Mater. Express*, 2016, **6**, 3097–3108.
14 J. Zhang, N. Riesen and H. Riesen, Mechanochemically Prepared SrFCl Nanophosphor Co-Doped With Yb^{3+} and Er^{3+} for Detecting Ionizing Radiation by Upconversion Luminescence, *Nanoscale*, 2017, **9**, 15958–15966.
15 J. Zhang and H. Riesen, Controlled Generation of Tm^{2+} Ions in Nanocrystalline BaFCl:Tm^{3+} by X-ray Irradiation, *J. Phys. Chem. A*, 2017, **121**, 803–809.

16 N. Riesen, C. Priest, D. G. Lancaster, K. Badek and H. Riesen, Ultra-High-Resolution Greyscale Fluorescence Images via UV-Exposure of Thin Flexible Phosphor Films, *Nanoscale*, 2023, **15**, 4863–4869.
17 N. T. Manamperi and F. A. Rabuffetti, UVC-Induced Valence Switching in BaFBr:Sm^{3+} Nanoplates, *J. Mater. Chem. C*, 2026, **14**, 4646–4657.
18 M. A. Stevens-Kalceff, Z. Liu and H. Riesen, Cathodoluminescence Microanalysis of Irradiated Microcrystalline and Nanocrystalline Samarium Doped BaFCl, *Microsc. Microanal.*, 2012, **18**, 1229–1238.
19 X. Wang and H. Riesen, Mechanochemical Synthesis of an Efficient Nanocrystalline BaFBr:Eu^{2+} X-ray Storage Phosphor, *RSC Adv.*, 2015, **5**, 85506–85510.
20 E. Aboelezz and B. W. Pogue, Review of Nanomaterial Advances for Ionizing Radiation Dosimetry, *Appl. Phys. Rev.*, 2023, **10**, 021312.
21 N. T. Manamperi, S. W. Sivirathne, A. M. Erlenbeck, S. Sameera Perera and F. A. Rabuffetti, Luminescence of Nanocrystalline BaFCl Codoped with $Eu^{2+/3+}$ and Tb^{3+}, *Dalton Trans.*, 2024, **53**, 16367–16376.
22 W. Chen, S. Wang, S. L. Westcott, J. Zhang, K. Dou, A. G. Joly and D. E. McCready, Structure and Luminescence of BaFBr:Eu^{2+} and BaFBr:Eu^{2+},Tb^{3+} Phosphors and Thin Films, *J. Appl. Phys.*, 2005, **97**, 083506.
23 M. Secu, C. Secu, V. Vasile, D. Predoi and D. Gazdaru, Time-Resolved Luminescence Spectroscopy of Eu^{2+} in BaFCl:Eu^{2+} X-ray Storage Phosphor, *J. Optoelectron. Adv. Mater.*, 2007, **9**, 1800–1802.
24 J. P. Spoonhower and M. S. Burberry, Time-Resolved Spectroscopy of BaFBr:Eu^{2+}, *J. Lumin.*, 1989, **43**, 221–226.
25 J. Sytsma and G. Blasse, Comparison of the Emission of Eu^{2+} in MFCl (M = Sr, Ba) and Gd^{3+} in YOCl, *J. Lumin.*, 1992, **51**, 283–292.
26 A. Meijerink and G. Blasse, Luminescence and Temperature Dependent Decay Behaviour of Divalent Europium in $Ba_5SiO_4X_6$ (X = Cl, Br), *J. Lumin.*, 1990, **47**, 1–5.
27 H. M. Rietveld, Line Profiles of Neutron Powder-Diffraction Peaks for Structure Refinement, *Acta Crystallogr.*, 1967, **22**, 151–152.
28 H. M. Rietveld, A Profile Refinement Method for Nuclear and Magnetic Structures, *J. Appl. Crystallogr.*, 1969, **2**, 65–71.
29 B. H. Toby and R. B. Von Dreele, GSAS-II: The Genesis of a Modern Open-Source All-Purpose Crystallography Software Package, *J. Appl. Crystallogr.*, 2013, **46**, 544–549.
30 P. Kubelka and F. Munk, Ein Beitrag zur Optik der Farbanstriche, *Z. Technol. Phys.*, 1931, **12**, 593–601.
31 J. L. Sommerdijk, J. M. P. J. Verstegen and A. Bril, Luminescence of MeFX:Eu^{2+} (Me = Sr, Ba; X = Cl, Br), *J. Lumin.*, 1974, **8**, 502–506.
32 T. Kobayasi, S. Mroczkowski, J. F. Owen and L. H. Brixner, Fluorescence Lifetime and Quantum Efficiency for $5d \rightarrow 4f$ Transitions in Eu^{2+} Doped Chloride and Fluoride Crystals, *J. Lumin.*, 1980, **21**, 247–257.
33 G. K. Liu, X. Y. Chen and J. Huang, Intensity and Bandwidth of Multiphonon Vibronic Transitions of Rare-Earth Ions in Crystals, *Mol. Phys.*, 2003, **101**, 1029–1036.
34 W. Chen, N. Kristianpoller, A. Shmilevich, D. Weiss, R. Chen and M. Su, X-ray Storage Luminescence of BaFCl:Eu^{2+} Single Crystals, *J. Phys. Chem. B*, 2005, **109**, 11505–11511.
35 S. Hesse, J. Zimmermann, H. von Seggern, X. Meng, C. Fasel and R. Riedel, Synthesis and Functionality of the Storage Phosphor BaFBr:Eu^{2+}, *J. Appl. Phys.*, 2009, **105**, 063505.
36 Q. Liang, Z. Li, W. Ma, Y. Shi and X. Yang, Controlled Synthesis and Optical Properties of BaFBr:Eu^{2+} Crystals via Ethanol/Water Solutions, *Mater. Res. Bull.*, 2012, **47**, 2357–2363.
37 J. Olchowka, H. Hagemann, T. Delgado and C. Wickleder, The Influence of Ionothermal Synthesis Using $BmimBF_4$ as a Solvent on Nanophosphor BaFBr:Eu^{2+} Photoluminescence, *Nanoscale*, 2018, **10**, 19706–19710.
38 T. Yanagida, H. Fukushima, G. Okada and N. Kawaguchi, Scintillation Properties of Eu:BaFBr Crystal, *Phys. B*, 2018, **550**, 21–25.
39 W.-D. Schneider, C. Laubschat, I. Nowik and G. Kaindl, Shake-up Excitations and Core–Hole Screening in Eu Systems, *Phys. Rev. B: Condens. Matter Mater. Phys.*, 1981, **24**, 5422–5425.
40 R. Vercaemst, D. Poelman, R. L. Van Meirhaeghe, L. Fiermans, W. H. Laflère and F. Cardon, An XPS Study of the Dopants' Valence States and the Composition of $CaS_{1-x}Se_x$:Eu and $SrS_{1-x}Se_x$:Ce Thin Film Electroluminescent Devices, *J. Lumin.*, 1995, **63**, 19–30.
41 F. Mercier, C. Alliot, L. Bion, N. Thromat and P. Toulhoat, XPS Study of Eu(III) Coordination Compounds: Core Levels Binding Energies in Solid Mixed Oxocompounds $Eu_mX_xO_y$, *J. Electron Spectrosc. Relat. Phenom.*, 2006, **150**, 21–26.
42 H. von Seggern, T. Voigt, W. Knüpfer and G. Lange, Physical Model of Photostimulated Luminescence of X-ray Irradiated BaFBr:Eu^{2+}, *J. Appl. Phys.*, 1988, **64**, 1405–1412.
43 Q. Ju, Y. Liu, R. Li, L. Liu, W. Luo and X. Chen, Optical Spectroscopy of Eu^{3+}-Doped BaFCl Nanocrystals, *J. Phys. Chem. C*, 2009, **113**, 2309–2315.
44 R. S. Eachus, W. G. McDugle, R. H. D. Nuttall, M. T. Olm, F. K. Koschnick, T. Hangleiter and J. M. Spaeth, Radiation-Produced Electron and Hole–Centers in Oxygen-Containing BaFBr: I. EPR and ODEPR Studies, *J. Phys.: Condens. Matter*, 1991, **3**, 9327–9338.
45 R. S. Eachus, W. G. McDugle, R. H. D. Nuttall, M. T. Olm, F. K. Koschnick, T. Hangleiter and J. M. Spaeth, Radiation-Produced Electron and Hole–Centers in Oxygen-Containing BaFBr: II. An ENDOR Study of OF^-, *J. Phys.: Condens. Matter*, 1991, **3**, 9339–9349.
46 T. J. Bastow, S. N. Stuart, W. G. McDugle, R. S. Eachus and J. M. Spaeth, Oxygen Impurities in X-ray Storage Phosphors BaFBr and BaFCl Investigated by ^{17}O NMR, *J. Phys.: Condens. Matter*, 1994, **6**, 8633–8644.

47 F. K. Koschnick, T. Hangleiter, K. S. Song and J. Spaeth, Optically Detected Magnetic Resonance Study of an Oxygen–Vacancy Complex in BaFBr, *J. Phys.: Condens. Matter*, 1995, **7**, 6925–6937.
48 T. Hangleiter, F. K. Koschnick, J. M. Spaeth, R. H. D. Nuttall and R. S. Eachus, Temperature Dependence of the Photostimulated Luminescence of X-Irradiate BaFBr:Eu^{2+}, *J. Phys.: Condens. Matter*, 1990, **2**, 6837–6846.
49 A. Ohnishi, K. Kan'no, Y. Iwabuchi and N. Mori, Recombination Luminescence From Self-Trapped Excitons in BaFBr, *Nucl. Instrum. Methods Phys. Res., Sect. B*, 1994, **91**, 210–214.
50 E. Radzhabov and V. Otroshok, Optical Spectra of Oxygen Defects in BaFCl and BaFBr Crystals, *J. Phys. Chem. Solids*, 1995, **56**, 1–7.
51 T. Kurobori, M. Liu and Y. Hirose, Temperature Dependence of the Near-IR Emission and Its Absorption in Oxygen-Doped BaFBr Crystals, *Jpn. J. Appl. Phys.*, 2001, **40**, L642–L645.
52 P. Kisliuk, H. H. Tippins, C. A. Moore and S. A. Pollack, Optical Spectrum and Zeeman Effect of CaF_2:Eu^{2+}, *Phys. Rev.*, 1968, **171**, 336–342.
53 T. Tsuboi and P. Silfsten, The Lifetime of Eu^{2+} Fluorescence in CaF_2:Eu^{2+} Crystals, *J. Phys.: Condens. Matter*, 1991, **3**, 9163–9167.
54 C. K. Duan, A. Meijerink, R. J. Reeves and M. F. Reid, The Unusual Temperature Dependence of the Eu^{2+} Fluorescence Lifetime in CaF_2 Crystals, *J. Alloys Compd.*, 2006, **408–412**, 784–787.
55 P. P. Feofilov and M. N. Tolstoi, Luminescence Kinetics of Divalent Samarium in Single Crystals of Strontium and Barium Fluorides, *Opt. Spektrosk.*, 1962, **13**, 294–296.
56 A. Meijerink, J. Nuyten and G. Blasse, Luminescence and Energy Migration in (Sr, Eu) B_4O_7, A System With a $4f^7$–$4f^6 5d$ Crossover in the Excited State, *J. Lumin.*, 1989, **44**, 19–31.
57 M. C. Downer, C. D. Cordero-Montalvo and H. Crosswhite, Study of New $4f^7$ Levels of Eu^{2+} in CaF_2 and SrF_2 Using Two-Photon Absorption Spectroscopy, *Phys. Rev. B: Condens. Matter Mater. Phys.*, 1983, **28**, 4931–4943.